How to cite: *Angew. Chem. Int. Ed.* **2023,** *62,* e202213962
International Edition: doi.org/10.1002/anie.202213962
German Edition: doi.org/10.1002/ange.202213962

Li-ion Conductors

Lithium-ion Mobility in $Li_6B_{18}(Li_3N)$ and Li Vacancy Tuning in the Solid Solution $Li_6B_{18}(Li_3N)_{1-x}(Li_2O)_x$

*Tassilo M. F. Restle, Lavinia Scherf, Jasmin V. Dums, Alexander G. Mutschke, Robert J. Spranger, Holger Kirchhain, Antti J. Karttunen, Leo van Wüllen, and Thomas F. Fässler**

Abstract: All-solid-state batteries are promising candidates for safe energy-storage systems due to non-flammable solid electrolytes and the possibility to use metallic lithium as an anode. Thus, there is a challenge to design new solid electrolytes and to understand the principles of ion conduction on an atomic scale. We report on a new concept for compounds with high lithium ion mobility based on a rigid open-framework boron structure. The host–guest structure $Li_6B_{18}(Li_3N)$ comprises large hexagonal pores filled with $^1_\infty[Li_7N]$ strands that represent a perfect cutout from the structure of α-Li_3N. Variable-temperature ^{7}Li NMR spectroscopy reveals a very high Li mobility in the template phase with a remarkably low activation energy below 19 kJ mol^{-1} and thus much lower than pristine Li_3N. The formation of the solid solution of $Li_6B_{18}(Li_3N)$ and $Li_6B_{18}(Li_2O)$ over the complete compositional range allows the tuning of lithium defects in the template structure that is not possible for pristine Li_3N and Li_2O.

Introduction

In order to run on renewable energy, mobile applications such as electronic devices and electric vehicles require safe and lightweight batteries. Currently, lithium ion batteries (LIBs) are widely used for this purpose because they are characterized by large gravimetric and volumetric capacities.[1] However, the combination of reactive inorganic species, large voltages and organic electrolytes as well as the possibility of short circuits by dendrite formation still pose significant safety issues. Therefore, solid-state batteries in which the liquid organic electrolytes are replaced by solid electrolytes have become a major focus of LIB research.[2]

Quite a large variety of crystalline systems have been investigated in the last two decades. Many of these can be assigned either to oxidic perovskite type structures,[3] garnet-type structures,[4] sodium super-ionic conductors (NASICON)-type structures[5] and lithium super-ionic conductor (LISICON)-type structures[6]) or sulfidic materials (thio-LISICON-type structures, thiophosphates[7] and lithium argyrodites[8]), and recently we introduced phosphide-based super-ionic conductors as a new material class.[9] Apart from these major classes, lithium hydrides,[10] lithium halides[11] and lithium nitride[12] have also been studied. Especially single crystalline Li_3N has long been known to offer a very high ionic conductivity above 10^{-3} S cm^{-1},[13] however, the bulk conductivity of 10^{-5} S cm^{-1} together with the low decomposition voltage limit its use.

Solid electrolytes with a high concentration of vacancies and a rigid open framework structure with channels in which the cation can move are ideal prerequisites for a successful Li ion conductor. A well-defined porous architecture that allows Li ions to be stored and reversibly inserted established metal–organic frameworks (MOFs)[14] and covalent organic frameworks (COFs)[15] as materials to be explored for developing all-solid-state electrolytes for Li ion batteries. Frameworks that are constructed from covalently linked building units to form two- or three-dimensional periodic architectures are expected to be more stable. Among open framework structures, carbon-, silicon- and boron-based materials are the most stable representatives, since the frameworks consist of three-dimensional covalently connected atoms. Open frameworks of these elements have been realized and predicted,[16] and for silicon various open frameworks have been discussed as anode materials through the possibility of lithium insertion.[17] We have recently reported on the ternary compound $LiBSi_2$ comprising a framework with B and Si atoms forming an ordered open framework structure with boron exclusively engaged in heteronuclear B–Si contacts and with encapsulated Li atoms

[*] T. M. F. Restle, L. Scherf, J. V. Dums, A. G. Mutschke, T. F. Fässler
Department of Chemistry, Technische Universität München
Lichtenbergstraße 4, 85747 Garching (Germany)
E-mail: thomas.faessler@lrz.tum.de
R. J. Spranger, H. Kirchhain, L. van Wüllen
Institute of Physics, Augsburg University
Universitätsstraße 1, 86159 Augsburg (Germany)
A. J. Karttunen
Department of Chemistry and Materials Science
Aalto University
00076 Aalto (Finland)
T. M. F. Restle
TUMInt.Energy Research GmbH
Lichtenbergstraße 4, 85747 Garching (Germany)

as the guest species.[18] However, covalent framework structures[19] that host lithium ion conductors are unknown.

Therefore, we extended our study on B and Si based framework compounds towards bare boron based open-framework structures in which Li_2O and $LiBH_4$ serve as a templates (*Tp*). In $Li_6B_{18}(Tp)_x$ covalently interconnected B_6 octahedra form three- and six-membered rings in the *ab* plane of the crystallographic unit cell with the B_6 octahedra acting as vertices (Figure 1a). The layers are stacked along the *c* direction in a primitive fashion with covalent B–B bonds between B_6 octahedra of adjacent layers. Small and large pores of the structure, which run along the *c* direction, are filled with Li as well as O atoms and BH_4 units, respectively.[20] $Li_6B_{18}(Tp)_x$ is structurally related to tetragonal Li_2B_6[21] and the cubic MB_6 compounds (Figure 1b and c, respectively),[22] which forms in absence of a template species under otherwise similar conditions. The existence of the very stable cubic MB_6 structure for monovalent (KB_6),[23] divalent (e.g., MgB_6, CaB_6),[22,24] trivalent (e.g., LaB_6, YB_6),[22] and even mixed-valent (SmB_6)[25] metals *M* demonstrate the structural and electronic flexibility of the boron framework. Electronic structure calculations suggest semiconducting behavior for the electron-precise hexaborides with divalent cations, whereas the electron-deficient or excess-electron hexaborides should be metallic.[26]

Here we report on the synthesis and structural characterization of the first combination of an open framework boron structure using the lithium ion conductor Li_3N as a template. Crystalline $Li_6B_{18}(Li_3N)_x$ ($x<1$) has an exceptionally low activation energy for lithium ion mobility, as shown by solid-state NMR spectroscopic methods. $Li_6B_{18}(Li_3N)_x$ combines the very stable open-framework structure of $Li_6B_{18}(Tp)_x$ with the outstanding Li ion conduction properties of Li_3N. Electronic band structure calculations on fully occupied $Li_6B_{18}(Li_3N)$ reveal semiconducting behavior. In order to test the possibility of tuning lithium defects we investigated the solid solutions of $Li_6B_{18}(Li_3N)$ and $Li_6B_{18}(Li_2O)$. Whereas the solid solution $(Li_3N)_{1-x}(Li_2O)_x$ is not known, the solid solution $Li_6B_{18}(Li_3N)_{1-x}(Li_2O)_x$ covers the complete compositional range, and samples for $x=0$, 0.25, 0.5, 0.75, and 1 have been synthesized and characterized.

Results and Discussion

Synthesis and characterization of polycrystalline $Li_6B_{18}(Li_3N)$ and $Li_6B_{18}(Li_2O)$

All experimental details are given in the Supporting Information. We have synthesized $Li_6B_{18}(Li_3N)$ using Li_3N as the template species from elemental Li, B and Li_3N. Using crystalline boron resulted in long needles of the product, however, with larger amounts of side phases (Supporting Information, Figures S2 and S4). In contrast to the reported synthesis of $Li_6B_{18}(Li_2O)$[20] we used nano-boron, and a slight sub-stoichiometric amount of lithium and a slight excess of Li_3N. The products with the smallest amount of impurities were obtained by using a ratio of Li/B/Li_3N = 5/18/1.2, where only 2.9(4) % of Li_2B_6 and small amount of another unknown impurity were detected. In order to have comparable synthesis conditions we reproduced the synthesis of $Li_6B_{18}(Li_2O)_x$ using also nano boron. The reaction carried out with Li_2O in place of Li_3N (Li/B/Li_2O = 6/18/1) resulted in $Li_6B_{18}(Li_2O)$ together with 2.3(1) % Li_2O as an impuritiy. $Li_6B_{18}(Li_3N)$ and $Li_6B_{18}(Li_2O)$ are obtained as red and orange powders, respectively (Supporting Information, Figure S1).

The PXRD patterns of the resulting products $Li_6B_{18}(Li_3N)_x$ and $Li_6B_{18}(Li_2O)_x$ show a slight shift of the template phase reflections, suggesting different unit cell sizes for the structures crystallizing in space group *P6/mmm*. Incorporation of the larger Li_3N unit in $Li_6B_{18}(Li_3N)_x$ gives rise to larger lattice parameters. Rietveld analyses were performed using the single crystal data of $Li_6B_{18}(Li_2O)$ as a starting model (Supporting Information Table S0 and Figure S0). The complete Rietveld data are listed in Tables S1–S3 (Supporting Information).

The crystal structure of $Li_6B_{18}(Li_3N)$ is depicted in Figure 2. The structure is built up by three-dimensional

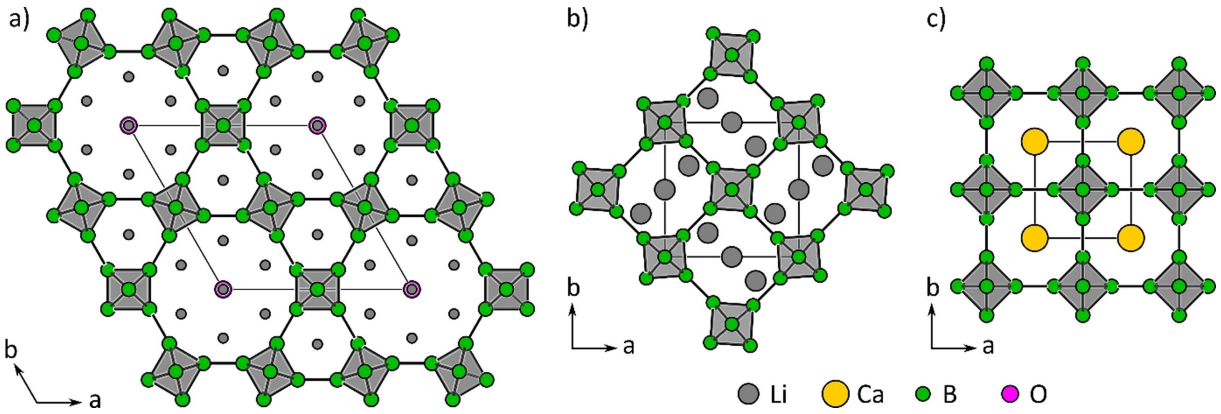

Figure 1. a) Hexagonal open framework structure of $Li_6B_{18}(Li_2O)_{0.26}$. The boron octahedra form a $3^24^86^2$ network in which the lithium and oxygen positions are located in the channels.[20] b) Tetragonal 4^{12} structure of Li_2B_6 comprising only small channels.[21] c) Cubic 4^{12} structure of CaB_6 and related rare earth metal borides.[27]

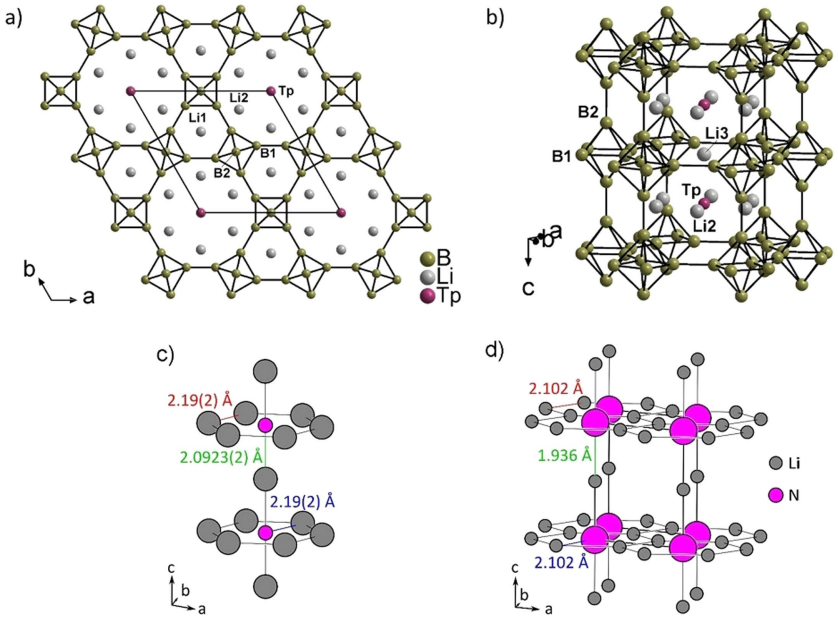

Figure 2. Crystal structure of $Li_6B_{18}(Li_3N)$. a) View along the *c* axis. The interconnected B_6 octahedra form a network featuring large hexagonal channels centered by N atoms. b) Side view towards the hexagonal pore. c) Depiction of the Li_7N formula unit located inside the large hexagonal pores of $Li_6B_{18}(Li_3N)$. d) Structure detail of α-Li_3N.[13] B, Li and *Tp* = N atoms are depict as green, grey and pink spheres, respectively.

interconnected B_6 octahedra comprising two boron positions. B1 represent the four atoms of a distorted square of the octahedra in the *ab* plane, and the B2 atoms are the caps above and below the plane completing the octadedra. The resulting interconnected B_6 octahedra form a 3636 Kagomé net in the *ab* plane, and the hexagonal primitive stacking of these planes results in two different kinds of channels along *c*. The smaller channels formed by three interconnected B_6 octahedra host the Li1 atoms. The larger channels formed by six interconnected B_6 octahedra are centered by the template N atoms, surrounded by the six-fold crystallographic site occupied by the Li2 atoms. The N atoms alternate with Li3 atoms along the *c* direction, resulting in a 6+2 coordination of N by Li atoms.

Most interestingly the content of the template in the hexagonal channels matches exactly the structural details of α-Li_3N. There are six Li atoms forming a hexagon with the N atom in the center and two lithium atoms located above and below the N atom, resulting in a strand with composition $_\infty^1[Li_7N]$. However, whereas in α-Li_3N the six Li atoms of the hexagon coordinate to three neigboring N atoms ($Li_3N = {}_\infty^1[Li(Li_{6/3}N])$, the strands in $Li_6B_{18}(Li_3N)_x$ are disjoint through the open boron framework. Consequently, the formula in the strands corresponds to $_\infty^1[Li_7N]$, and thus, the content is Li richer (Figures 2c and d).

The structure is closely related to that of $Li_6B_{18}(Li_2O)_x$. As pointed out before, the proportion of Li_2O is subject to change, and the amount of templated Li_2O grows with an increasing amount of Li_2O used for the synthesis.[20] According to Rietveld refinements the occupation of the template N and O atoms never reaches a full occupancy, but arises to 84(2) % for N in $Li_6B_{18}(Li_3N)$ and 90.7(7) % for O in $Li_6B_{18}(Li_2O)$. For the novel compound with *Tp* = N, EDX measurements confirm the presence and the amount of nitrogen according to the partial occupation obtained from the Rietveld refinement (Supporting Information, Figure S7, Table S3).

NMR characterization and Li ion mobility in $Li_6B_{18}(Li_3N)$

Since the samples are rather air sensitive, all sample handling has to be performed in a glovebox with Argon atmosphere. The ^{7}Li MAS NMR spectrum of $Li_6B_{18}(Li_3N)$ taken at room temperature exhibits a single ^{7}Li signal at 2.3 ppm. The ^{11}B MAS NMR spectrum shows a single, slightly asymmetric signal at 5.0 ppm (Figure 3). After a few seconds of exposure to air, a drastic color change (from orange-brown to grey-green) is observed, and the ^{7}Li MAS NMR spectrum now shows two signals at 2.4 and −5.2 ppm. Corresponding changes are observed in the ^{11}B MAS NMR spectra, now featuring two signals at 5.0 and 25 ppm. From the spread and the intensity of the spinning sidebands in the ^{11}B MAS NMR spectrum, a quadrupolar coupling constant of 1.1 MHz can be deduced (Supporting Information, Figure S8).

In order to check for a possible Li dynamic we determined the evolution of the static ^{7}Li NMR linewidth and the ^{7}Li T_1 relaxation time with temperature for the $Li_6B_{18}(Li_3N)$ sample. The ^{7}Li NMR spectra as a function of temperature are shown in Figure 4. For the I = 3/2 nucleus ^{7}Li, the overall static linewidth equals the magnitude of the quadrupolar interaction represented by the quadrupolar coupling constant C_Q, which is related to the principal component of the electric field gradient (EFG), V_{ZZ} via $C_Q = eQV_{ZZ}/h$, with e denoting the elementary charge, and

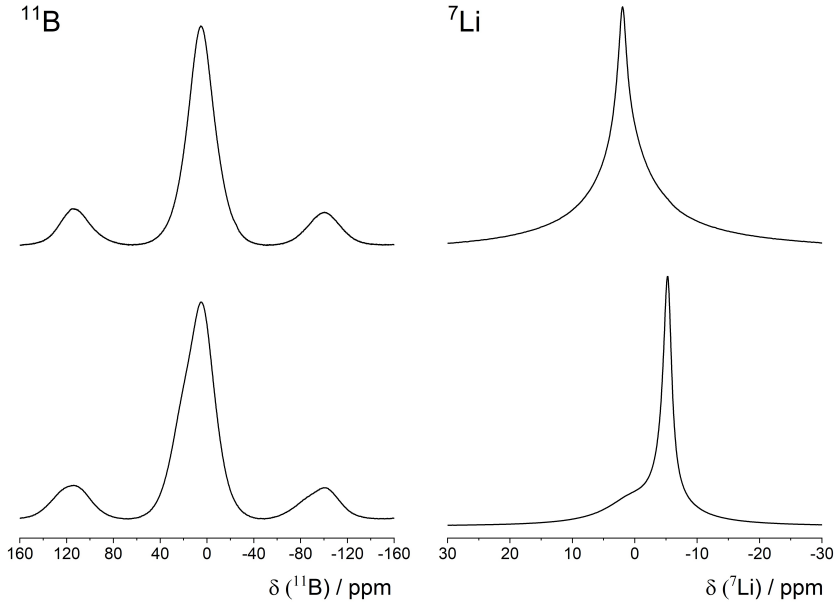

Figure 3. ^{11}B-MAS (left) and ^{7}Li-MAS (right) NMR spectra of $Li_6B_{18}(Li_3N)$: top spectra: sample kept under inert conditions; bottom spectra: sample exposed to air.

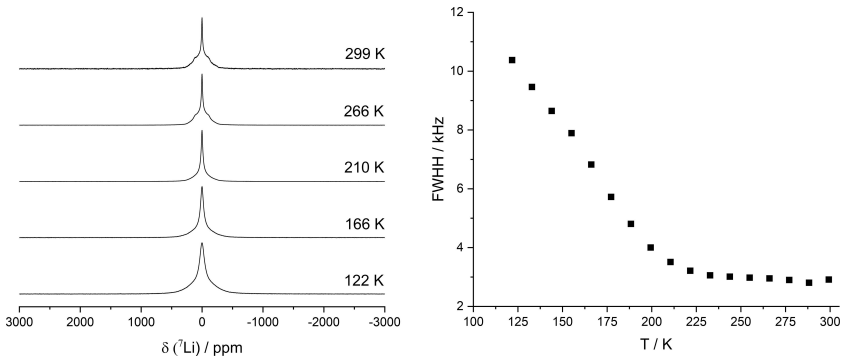

Figure 4. ^{7}Li-solid-echo spectra (left) and the ^{7}Li line width, determined as full width at half height of the central transition (right), as a function of temperature for $Li_6B_{18}(Li_3N)$.

Q the quadrupole moment (for ^{7}Li: $4.0\times10^{-30}\,m^2$). In the room temperature ^{7}Li spectrum, the narrow central line represents the $m=1/2\rightarrow m=-1/2$ central transition, whereas the remaining signal comprises the two satellite transitions $m=\pm1/2\rightarrow\pm3/2$. A simulation employing the DMFIT[28] software produces a quadrupolar coupling constant $C_Q=$ 54 kHz and an asymmetry parameter $\eta_Q=0$. The line width of the central transition is not affected by the quadrupolar interaction and therefore is governed by the homo (^{7}Li-^{7}Li) and heteronuclear (^{7}Li-^{11}B) dipolar interactions, which both exhibit an orientational dependence scaling with the second Legendrian. In the absence of any motional processes (rigid regime) this entails a broadening of the signals. Any motional process, however, will result in an at least partial averaging of the interactions entailing a narrowing of the line width of the central transition. Although the measurements extend to temperatures as low as 122 K, no characteristic low-temperature plateau (rigid regime) is observed. Instead, the line width continuously decreases until $T=$ 220 K and then reaches the motional narrowing plateau. Thus, the evolution of the line width with temperature clearly indicates the presence of a rather low activated dynamic process. Since the rigid lattice regime is not reached, we can only give an upper value for the activation energy employing the Waugh Fedin relation of $E_A=0.156\,T_{onset}$, taking the lowest accessed temperature as the onset temperature T_{onset}. This gives $E_A<19\,kJ\,mol^{-1}$. An alternative approach to determine the activation energy relies on the analysis of the temperature dependence of the spin lattice relaxation time T_1, which was measured employing a standard inversion recovery sequence. The resulting T_1 data is collected in Figure 5. An analysis of the data using the BPP-model[29] (Bloembergen, Purcell, Pound) produces an activation energy of 6.6 kJ mol^{-1}. However, since the data is dominated by the low-temperature portion of the BPP curve, and it is well known that the low-temperature data of

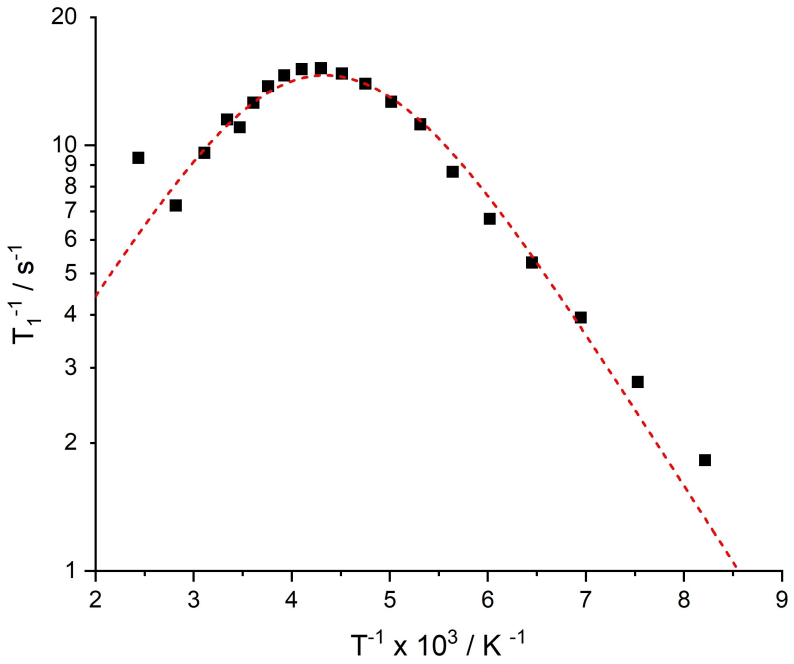

Figure 5. ^{7}Li-T_1 NMR spectroscopy data for $Li_6B_{18}(Li_3N)$. Experimental data points are shown as black squares. The red dashed line corresponds to a simulation of the data employing a BPP model for the low-temperature process, resulting in values of $C_1 = 7.5 \times 10^9\ s^{-2}$, $\tau_C^0 = 2.6 \times 10^{-11}$ s, $E_{A,1} = 6.6\ kJ\ mol^{-1}$.

T_1 curves are often biased to lower values, this value marks the lower boundary of the activation energy. Combining the results of the line shape analysis and T_1 data we come to the conclusion that $6.6\ kJ\ mol^{-1} < E_A < 19\ kJ\ mol^{-1}$, which is a remarkably low value and renders these open-framework materials interesting for solid electrolyte applications. A detailed evaluation of the mechanism of ion transport within these phases is beyond the scope of this contribution and will be presented elsewhere.

Electronic structure of $Li_6B_{18}(Li_3N)$.

The electronic structure of the open-framework structure was analyzed with quantum chemical methods at the DFT-HSE06/TZVP level of theory, assuming full occupation of all atomic positions in $Li_6B_{18}(Li_3N)$. The optimized lattice parameters are $a = 8.216$ Å and $c = 4.109$ Å, deviating only by 0.7 % and 1.8 % from the experimental lattice parameters, respectively. Harmonic frequency calculations on the optimized crystal structure result in a relatively small imaginary mode of $-82\ cm^{-1}$. This imaginary mode can be explained by the full occupation used for the N atom in the calculations, instead of the partial occupation in the experimental structure. A distortion of the structure along the imaginary mode and a subsequent structure optimization in a space group of lower symmetry led to an unreasonably large distortion of the structure.

The electronic band structure and the density of states of $Li_6B_{18}(Li_3N)$ are depicted in Figure 6. The band structure reveals the material to be a semiconductor with a direct band gap of 1.9 eV at the Γ point (Supporting Information, Figure S9 for a depiction of the Brillouin zone), rendering the structure type also as an interesting candidate for optoelectronic applications. The size of the band gap corresponds to the reddish color of the compound. Interestingly, the top valence bands between 0 and about −1.1 eV correspond mainly to atoms located inside the large pores of the open framework structure, as shown by the DOS curves. N has the largest contribution to the total DOS in this part, whereas it has almost no contribution at lower energies. Thus $Li_6B_{18}(Li_3N)$ represents a true host–guest compound.

Raman spectroscopy

Experimental Raman spectra for $Li_6B_{18}(Li_3N)$ are depicted in Figure 7. Based on the calculated spectra, which are in good agreement with the experimental ones, the strongest peaks 1 A_{1g}, 2 A_{1g} and 3 A_{1g} correspond to the known modes of the boron framework as described for MB_6.[30] Due to the more complex structure of $Li_6B_{18}(Li_3N)$ compared to cubic MB_6 more signals occur (Table S4). For each mode the unit cell contains three instead of one octahedral B_6 units, which can exhibit combinations of different vibrations and end up in a higher variation of modes. All vibrational modes are given in the Supporting Information (Figures S10 and S11). Experimental spectra of $Li_6B_{18}(Li_2O)$ show a significant difference to that of $Li_6B_{18}(Li_3N)$ which originates from the lower lithium content (Li_2O versus Li_3N) with more disorder on the Li sites. The corresponding Raman bands are slightly shifted to higher wave numbers, and shoulders arise.

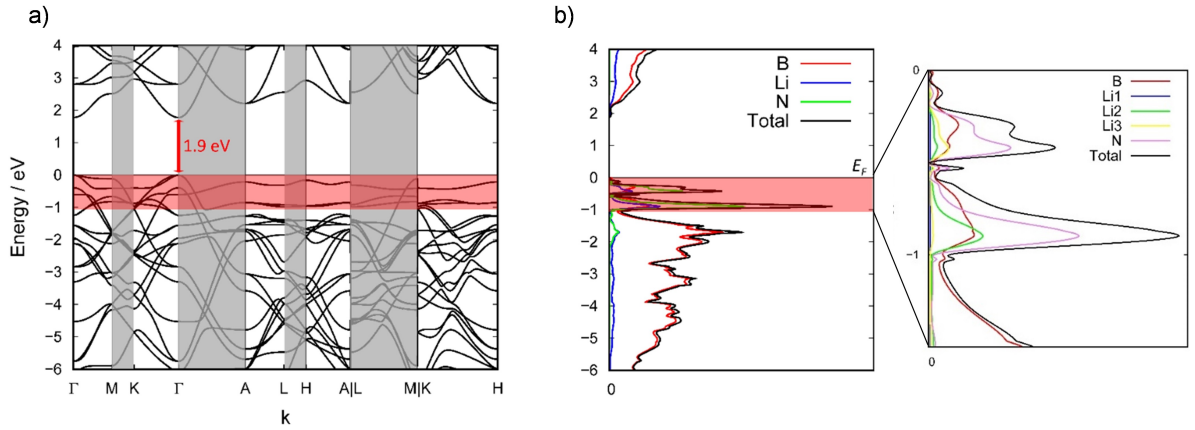

Figure 6. a) Band structure of $Li_6B_{18}(Li_3N)$ in the range of −6 eV to 4 eV; b) total and partial DOS curves with enlargement between −1.5 and 0 eV; bands marked in red mainly correspond to states of the atoms located in the large pores of the structure. The Fermi level E_F is set to 0 eV.

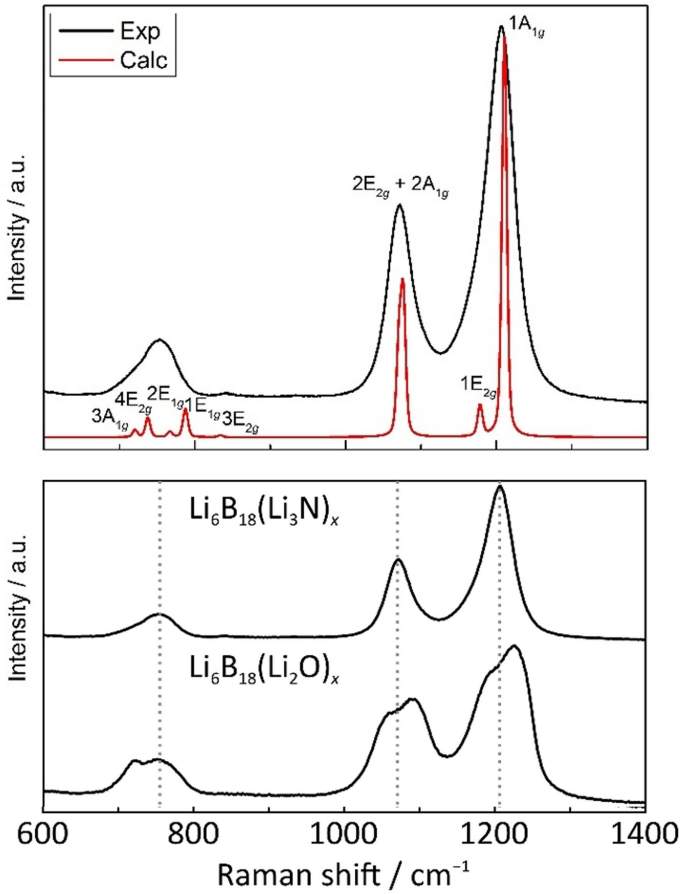

Figure 7. Raman spectra of $Li_6B_{18}(Li_3N)_x$ (experimental) in black and of $Li_6B_{18}(Li_3N)$ (calculated) in red with assigned modes (upper part) and $Li_6B_{18}(Li_2O)_x$ as well as for direct comparison that of $Li_6B_{18}(Li_3N)_x$ (lower part). The Raman shifts of $Li_6B_{18}(Li_3N)_x$ are marked by dotted lines. Exact Raman shifts are listed in Table S4 (Supporting Information).

Synthesis and characterization of the solid solutions $Li_6B_{18}(Li_3N)_{1-x}(Li_2O)_x$ ($x = 0.25, 0.50, 0.75$)

The products of the solid solution $Li_6B_{18}(Li_3N)_{1-x}(Li_2O)_x$ ($x = 0.25$, 0.50, 0.75, 1) were synthesized by heating of lithium, nano-boron and the template species in steel ampules at 1173 K. The results of a single crystal structure determination of $Li_6B_{18}(Li_2O)_x$ was used as initial structural model for the solid solution $Li_6B_{18}(Li_3N)_{1-x}(Li_2O)_x$ ($x = 0$, 0.25, 0.50, 0.75, 1). By increasing the amount of Li_2O, the color of the products change from red-brown to orange (Figure S1). The Li_3N-rich compounds contain small

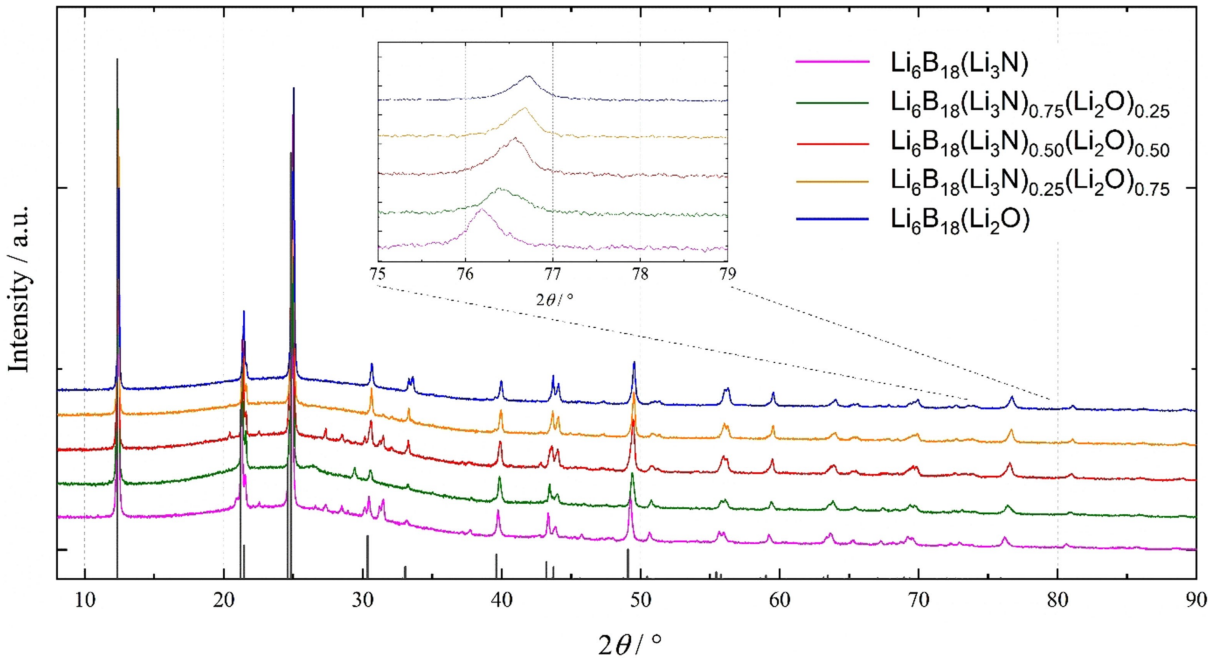

Figure 8. Experimental powder X-ray diffraction pattern of the solid solution $Li_6B_{18}(Li_3N)_{1-x}(Li_2O)_x$ ($x=0$, 0.25, 0.50, 0.75, 1). Especially at higher 2θ angles a shift of the reflections from lower angles in $Li_6B_{18}(Li_3N)$ to higher angles in $Li_6B_{18}(Li_2O)$ is observed. Black lines mark the reflections of Li_6B_{18}(*Tp*). In the PXRDs of $Li_6B_{18}(Li_3N)_{1-x}(Li_2O)_x$ ($x=0$, 0.25, 0.50) some unknown reflections occur, whereas $Li_6B_{18}(Li_3N)_{1-x}(Li_2O)_x$ ($x=0.75$) is phase-pure, and $Li_6B_{18}(Li_2O)$ exhibits only reflections of Li_2O as impurities.

amounts of unknown impurities, with weak reflections at around 30° 2θ. By contrast, the compound $Li_6B_{18}(Li_3N)_{0.25}(Li_2O)_{0.75}$ is phase pure according to the powder X-ray diffractogram. The solid solution $Li_6B_{18}(Li_3N)_{1-x}(Li_2O)_x$ ($0 \leq x \leq 1$) has no miscibility gap and crystallizes in the hexagonal space group *P6/mmm*.

From $Li_6B_{18}(Li_3N)$ to $Li_6B_{18}(Li_2O)$ the reflections are shifted to higher 2θ angles, which is shown for higher 2θ angles in Figure 8. Cell parameters of the solid solution $Li_6B_{18}(Li_3N)_{1-x}(Li_2O)_x$ ($x=0$, 0.25, 0.50, 0.75, 1) obtained from indexing of the reflections of the experimental powder X-ray diffraction patterns are given in Table 1. The correlation of the cell parameter with x is not linear and therefore not fully in accordance with Vegard's law. From $Li_6B_{18}(Li_3N)$ to $Li_6B_{18}(Li_2O)$ the cell parameter c decreases almost linearly, whereas a and therefore also the volume V decreases exponentially (Supporting Information, Figure S12).The cell parameters determined from Rietveld refinements follow the same trend (Supporting Information, Table S1). The anisotropic changes might be related to the lithium vacancies created in the structure by the substitution of Li_3N by Li_2O. With increasing x and partial substitution of N by O template atoms, the lithium content decreases, since according to Rietveld refinements the occupation of the Li2 position changes, whereas other positions remain fully occupied (Supporting Information, Table S2), and the Li2 atoms are all located in the *ab* plane. EDX measurements confirm the presence of N in the solid solution $Li_6B_{18}(Li_3N)_{1-x}(Li_2O)_x$ ($x=0.25$, 0.50, 0.75, 1.0) (Figure S13). For $x=0$ and 0.25 the amount of N measured by EDX is in very good agreement with the partial occupation of the template species determined by Rietveld refinement (Table S3). For the solid solutions, rudiments of needles can be observed, although the formation of needles is much less pronounced as in the $Li_6B_{18}(Li_3N)$ sample (Supporting Information, Figure S14).

Table 1: Cell parameters of the solid solution $Li_6B_{18}(Li_3N)_{1-x}(Li_2O)_x$ ($x=$ 0, 0.25, 0.50, 0.75, 1) from indexing of the reflections of the experimental powder X-ray diffraction patterns.

x in $Li_6B_{18}(Li_3N)_{1-x}(Li_2O)_x$	a [Å]	c [Å]	V [Å3]
0[a]	8.2484(13)	4.1711(7)	245.77(5)
0.25	8.2285(23)	4.1610(12)	243.99(8)
0.50	8.220(3)	4.1499(15)	242.84(11)
0.75	8.2130(14)	4.1424(8)	241.99(6)
1[a]	8.2127(12)	4.1374(8)	241.67(5)

[a] value set to 0 = and 1, respectively.

Lithium rich ionic compounds are in principle interesting candidates for possible lithium ion conductors. Single crystalline α-Li_3N has been described with a high ionic conductivity above 10^{-3} S cm^{-1} parallel to the Li_2N planes,[13] but the bulk shows a conductivity of 10^{-5} S cm^{-1}. A major advantage for the design and improvement of high lithium ion mobility is the tuning of vacancies that allow for the mobility of ions. For examples shows the structurally related Li_3P rather low ionic conductivity[31] which however can be significantly increased by the formation of a solid solution with Li_2S and vice versa.[32] In a simplified picture the P atoms occupy the same positions of the cubic closest atom array of S atoms in the Li_2S structure type. For charge

compensation of the higher charged P atoms (P^{3-} versus S^{2-}) the number of Li atoms increases in the solid solution $(Li_3P)_x(Li_2S)_{1-x}$ with increasing x.

Solid solution of α-Li_3N and Li_2O are not reported, most probably due to the rather different crystal structures of the two boundary compounds. The rigid open-framework boron structure Li_6B_{18} allows hosting both Li_3N and Li_2O as templates and is thus capable to form a solid solution of the templates. We found in addition that the partial structure Li_3N in the host–guest structure $Li_6B_{18}(Li_3N)$ comprises $_\infty^1[Li_7N]$ strands in the large hexagonal pores of the host that represent a perfect cutout from the α-Li_3N structure. The template phase $Li_6B_{18}(Li_3N)$ and the solid solutions $Li_6B_{18}(Li_3N)_{1-x}(Li_2O)_x$ can be readily synthesized for $x=0$, 0.25, 0.5, 0.75, and 1 by the reaction of stoichiometric ratios of Li_3N/Li_2O with elemental Li and B.

Variable-temperature ^{7}Li NMR spectroscopy reveals a very high Li ion mobility in the template phase $Li_6B_{18}(Li_3N)$ with a remarkably low activation energy below 19 kJ mol^{-1}. Since the pristine compound shows already a rather high ionic conductivity the investigation of the $Li_6B_{18}(Li_3N)_{1-x}(Li_2O)_x$ might even improve this property. Since the structure hosts Li atoms at chemically rather different positions such as exclusively surrounded by B_6 octahedra and two positions in the vicinity of the N atom in perfect analogy to the structure of Li_3N, the compound also represents an interesting candidate to determine Li ion migration pathways. A study of the solid solution including theoretical and experimental determination of Li ion migration pathways is presented in a forthcoming paper.[33]

Supporting Information

Supporting Information includes experimental details of synthesis of $Li_6B_{18}(Li_3N)$, $Li_6B_{18}(Li_2O)$, $Li_6B_{18}(Li_3N)_{1-x}(Li_2O)_x$.with $x=0{,}25$, 0.50, and 0.75. Details of powder X-ray diffraction, Rietveld analysis, scanning electron microscopy, Raman spectroscopy, NMR spectroscopy, electronic structure calculations, and tables of crystallographic data of $Li_6B_{18}(Li_3N)$ and $Li_6B_{18}(Li_2O)$. Deposition Numbers 2207446 (for $Li_6B_{18}(Li_3N)$, 2207443 (for $Li_6B_{18}(Li_3N)_{0.75}(Li_2O)_{0.25}$), 2207447 (for $Li_6B_{18}(Li_3N)_{0.5}(Li_2O)_{0.5}$), 2207464 (for $Li_6B_{18}(Li_3N)_{0.25}(Li_2O)_{0.75}$), and 2207445 (for $Li_6B_{18}(Li_2O)$) contain the supplementary crystallographic data for this paper. These data are provided free of charge by the joint Cambridge Crystallographic Data Centre and Fachinformationszentrum Karlsruhe Access Structures service.

Acknowledgements

The authors are grateful to the Bavarian Ministry of Economic Affairs, Regional Development, and Energy for funding their research in the project "Industrialisierbarkeit von Festkörperelektrolytzellen". A.J.K. thanks CSC—the Finnish IT Center for Science for computational resources. Open Access funding enabled and organized by Projekt DEAL.

Conflict of Interest

The authors declare no competing financial interest.

Data Availability Statement

The data that support the findings of this study are available in the Supporting Information of this article.

Keywords: Boride · Host Guest System · Ion Conduction · Lithim · Nitride

[1] A. Patil, V. Patil, D. W. Shin, J. W. Choi, D. S. Paik, S. J. Yoon, *Mater. Res. Bull.* **2008**, *43*, 1913–1942.

[2] a) J. G. Kim, B. Son, S. Mukherjee, N. Schuppert, A. Bates, O. Kwon, M. J. Choi, H. Y. Chung, S. Park, *J. Power Sources* **2015**, *282*, 299–322; b) J. Janek, W. G. Zeier, *Nat. Energy* **2016**, *1*, 16141; c) J. C. Bachman, S. Muy, A. Grimaud, H. H. Chang, N. Pour, S. F. Lux, O. Paschos, F. Maglia, S. Lupart, P. Lamp, L. Giordano, Y. Shao-Horn, *Chem. Rev.* **2016**, *116*, 140–162; d) Z. Zhang, Y. Shao, B. Lotsch, Y.-S. Hu, H. Li, J. Janek, L. F. Nazar, C.-W. Nan, J. Maier, M. Armand, L. Chen, *Energy Environ. Sci.* **2018**, *11*, 1945–1976; e) M. V. Reddy, C. M. Julien, A. Mauger, K. Zaghib, *Nanomaterials* **2020**, *10*, 1606.

[3] a) Y. Inaguma, C. Liquan, M. Itoh, T. Nakamura, T. Uchida, H. Ikuta, W. Wakihara, *Solid State Commun.* **1993**, *86*, 689; b) Y. Inaguma, L. Q. Chen, M. Itoh, T. Nakamura, *Solid State Ionics* **1994**, *70*, 196–202; c) O. Bohnke, C. Bohnke, J. L. Fourquet, *Solid State Ionics* **1996**, *91*, 21–31; d) S. Stramare, V. Thangadurai, W. Weppner, *Chem. Mater.* **2003**, *15*, 3974–3990.

[4] a) R. Murugan, V. Thangadurai, W. Weppner, *Angew. Chem. Int. Ed.* **2007**, *46*, 7778–7781; *Angew. Chem.* **2007**, *119*, 7925–7928; b) Y. T. Li, J. T. Han, C. A. Wang, H. Xie, J. B. Goodenough, *J. Mater. Chem.* **2012**, *22*, 15357–15361; c) V. Thangadurai, S. Narayanan, D. Pinzaru, *Chem. Soc. Rev.* **2014**, *43*, 4714–4727.

[5] a) H. Aono, E. Sugimoto, Y. Sadaoka, N. Imanaka, G. Y. Adachi, *J. Electrochem. Soc.* **1989**, *136*, 590–591; b) A. Martínez-Juárez, C. Pecharromán, J. E. Iglesias, J. M. Rojo, *J. Phys. Chem. B* **1998**, *102*, 372–375.

[6] a) P. G. Bruce, A. R. West, *J. Electrochem. Soc.* **1983**, *130*, 662–669; b) A. D. Robertson, A. R. West, A. G. Ritchie, *Solid State Ionics* **1997**, *104*, 1–11; c) H. Y. P. Hong, *Mater. Res. Bull.* **1978**, *13*, 117–124; d) A. R. Rodger, J. Kuwano, A. R. West, *Solid State Ionics* **1985**, *15*, 185–198.

[7] a) R. Kanno, M. Maruyama, *J. Electrochem. Soc.* **2001**, *148*, A742–A746; b) R. Kanno, T. Hata, Y. Kawamoto, M. Irie, *Solid State Ionics* **2000**, *130*, 97–104; c) M. Murayama, R. Kanno, M. Irie, S. Ito, T. Hata, N. Sonoyama, Y. Kawamoto, *J. Solid State Chem.* **2002**, *168*, 140–148; d) A. Kuhn, R. Eger, J. Nuss, B. V. Lotsch, *Z. Anorg. Allg. Chem.* **2013**, *639*, 1087–1089; e) N. Kamaya, K. Homma, Y. Yamakawa, M. Hirayama, R. Kanno, M. Yonemura, T. Kamiyama, Y. Kato, S. Hama, K. Kawamoto, A. Mitsui, *Nat. Mater.* **2011**, *10*, 682–686; f) P. F. Zhou, J. B. Wang, F. Y. Cheng, F. J. Li, J. Chen, *Chem. Commun.* **2016**, *52*, 6091–6094.

[8] a) H.-J. Deiseroth, S.-T. Kong, H. Eckert, J. Vannahme, C. Reiner, T. Zaiss, M. Schlosser, *Angew. Chem. Int. Ed.* **2008**, *47*, 755–758; *Angew. Chem.* **2008**, *120*, 767–770; b) N. J. J. de Klerk, T. Roslon, M. Wagemaker, *Chem. Mater.* **2016**, *28*, 7955–7963; c) N. Minafra, S. P. Culver, T. Krauskopf, A. Senyshyn, W. G. Zeier, *J. Mater. Chem. A* **2018**, *6*, 645–651.

[9] a) T. M. F. Restle, C. Sedlmeier, H. Kirchhain, W. Klein, G. Raudaschl-Sieber, V. L. Deringer, L. van Wüllen, H. A. Gasteiger, T. F. Fässler, *Angew. Chem. Int. Ed.* **2020**, *59*, 5665–5674; *Angew. Chem.* **2020**, *132*, 5714–5723; b) S. Strangmüller, H. Eickhoff, D. Müller, W. Klein, G. Raudaschl-Sieber, H. Kirchhain, C. Sedlmeier, V. Baran, A. Senyshyn, V. L. Deringer, *J. Am. Chem. Soc.* **2019**, *141*, 14200–14209.
[10] M. Matsuo, S. Orimo, *Adv. Energy Mater.* **2011**, *1*, 161–172.
[11] H. D. Lutz, P. Kuske, K. Wussow, *Solid State Ionics* **1988**, *28*, 1282–1286.
[12] a) T. Lapp, S. Skaarup, A. Hooper, *Solid State Ionics* **1983**, *11*, 97–103; b) H. Yamane, S. Kikkawa, M. Koizumi, *Solid State Ionics* **1987**, *25*, 183–191; c) W. Schnick, J. Lucke, *Z. Anorg. Allg. Chem.* **1990**, *588*, 19–25; d) A. Rabenau, *Solid State Ionics* **1982**, *6*, 277–293.
[13] a) E. Zintl, G. Brauer, *Z. Elektrochem.* **1935**, *41*, 102–107; b) U. von Alpen, A. Rabenau, G. H. Talat, *Appl. Phys. Lett.* **1977**, *30*, 621.
[14] a) L. Wang, Y. Han, X. Feng, J. Zhou, P. Qi, B. Wang, *Coord. Chem. Rev.* **2016**, *307*, 361–381; b) J. Liu, X. Song, T. Zhang, S. Liu, H. Wen, L. Chen, *Angew. Chem. Int. Ed.* **2021**, *60*, 5612–5624; *Angew. Chem.* **2021**, *133*, 5672–5684.
[15] a) X. Li, K. P. Loh, *ACS Mater. Lett.* **2019**, *1*, 327–335; b) T. Sun, J. Xie, W. Guo, D.-S. Li, Q. Zhang, *Adv. Energy Mater.* **2020**, *10*, 1904199.
[16] a) R. Nesper, K. Vogel, P. E. Blöchl, *Angew. Chem. Int. Ed. Engl.* **1993**, *32*, 701–703; *Angew. Chem.* **1993**, *105*, 786–788; b) A. J. Karttunen, T. F. Fässler, M. Linnolahti, T. A. Pakkanen, *Inorg. Chem.* **2011**, *50*, 1733–1742; c) L. Fan, D. Yang, D. Li, *Materials* **2021**, *14*, 3964; d) I. A. Baburin, D. M. Proserpio, V. A. Saleev, A. V. Shipilova, *Phys. Chem. Chem. Phys.* **2015**, *17*, 1332–1338; e) D. Y. Kim, S. Stefanoski, O. O. Kurakevych, T. A. Strobel, *Nat. Mater.* **2015**, *14*, 169–173; f) T. Zeng, R. Hoffmann, R. Nesper, N. W. Ashcroft, T. A. Strobel, D. M. Proserpio, *J. Am. Chem. Soc.* **2015**, *137*, 12639–12652.
[17] a) P. Warrier, C. A. Koh, *Appl. Phys. Rev.* **2016**, *3*, 040805; b) T. Langer, S. Dupke, H. Trill, S. Passerini, H. Eckert, R. Pöttgen, M. Winter, *J. Electrochem. Soc.* **2012**, *159*, A1318–A1322.
[18] M. Zeilinger, L. van Wüllen, D. Benson, V. F. Kranak, S. Konar, T. F. Fässler, U. Häussermann, *Angew. Chem. Int. Ed.* **2013**, *52*, 5978–5982; *Angew. Chem.* **2013**, *125*, 6094–6098.
[19] a) L. Zhu, M. Borstad Gustav, H. Liu, A. Guńka Piotr, M. Guerette, J.-A. Dolyniuk, Y. Meng, E. Greenberg, B. Prakapenka Vitali, L. Chaloux Brian, A. Epshteyn, E. Cohen Ronald, A. Strobel Timothy, *Sci. Adv.* **2020**, *6*, eaay8361; b) J.-M. Hübner, W. Jung, M. Schmidt, M. Bobnar, P. Koželj, B. Böhme, M. Baitinger, M. Etter, Y. Grin, U. Schwarz, *Inorg. Chem.* **2021**, *60*, 2160–2167.
[20] M. Wörle, R. Nesper, G. Mair, H. G. von Schnering, *Solid State Sci.* **2007**, *9*, 459–464.
[21] G. Mair, H. G. von Schnering, M. Wörle, R. Nesper, *Z. Anorg. Allg. Chem.* **1999**, *625*, 1207–1211.
[22] F. Neumann, M. von Stackelberg, *Z. Phys. Chem. Abt. B* **1932**, *19*, 314–320.
[23] R. Naslain, J. Etourneau, *C. R. Seances Acad. Sci. Ser. C* **1966**, *263*, 484–487.
[24] H. Moissan, P. Williams, *C. R. Hebd. Seances Acad. Sci.* **1897**, *125*, 629–634.
[25] T. Kasuya, *Europhys. Lett.* **1994**, *26*, 283–287.
[26] a) P. G. Perkins, D. R. Armstrong, A. Breeze, *J. Phys. C* **1975**, *8*, 3558–3570; b) P. G. Perkins, A. V. J. Sweeney, *J. Less-Common Met.* **1976**, *47*, 165–173.
[27] M. von Stackelberg, F. Neumann, *Z. Phys. Chem. Abt. B* **1932**, *19*, 314–320.
[28] D. Massiot, F. Fayon, M. Capron, I. King, S. Le Calvé, B. Alonso, J.-O. Durand, B. Bujoli, Z. Gan, G. Hoatson, *Magn. Reson. Chem.* **2002**, *40*, 70–76.
[29] N. Bloembergen, E. M. Purcell, R. V. Pound, *Phys. Rev.* **1948**, *73*, 679–712.
[30] a) M. Ishii, M. Aono, S. Muranaka, S. Kawai, *Solid State Commun.* **1976**, *20*, 437–440; b) N. Ogita, S. Nagai, N. Okamoto, F. Iga, S. Kunii, T. Akamtsu, J. Akimitsu, M. Udagawa, *J. Solid State Chem.* **2004**, *177*, 461–465.
[31] a) G. Nazri, *Solid State Ionics* **1989**, *34*, 97–102; b) F. Wegner, F. Kamm, F. Pielnhofer, A. Pfitzner, *Z. Anorg. Allg. Chem.* **2022**, *648*, e202100358.
[32] C. Szczuka, B. Karasulu, M. F. Groh, F. N. Sayed, T. J. Sherman, J. D. Bocarsly, S. Vema, S. Menkin, S. P. Emge, A. J. Morris, C. P. Grey, *J. Am. Chem. Soc.* **2022**, *144*, 16350–16365.
[33] R. J. Spranger, H. Kirchhain, T. M. F. Restle, J. V. Dums, A. J. Karttunen, L. van Wüllen, T. F. Fässler, *J. Phys. Chem. C* **2023**, DOI: 10.1021/acs.jpcc.2c06839.

Manuscript received: September 21, 2022
Accepted manuscript online: January 1, 2023
Version of record online: January 24, 2023